Critical island-size, stability, and morphology of 2D colloidal Au nanoparticle islands

Bradley C. Hubartt and Jacques G. Amar
Department of Physics and Astronomy, University of Toledo, Toledo, Ohio 43606, USA

(Received 30 October 2014; accepted 15 December 2014; published online 12 January 2015)

The critical island-size, stability, and morphology of 2D colloidal Au nanoparticle islands formed during drop-drying are studied using an empirical potential which takes into account core-core, ligand-ligand, and ligand-solvent interactions. Good agreement with experiment is obtained for the dependence of the critical island-size on nanoparticle diameter. Our results for the critical length-scale for smoothing via edge-diffusion are also consistent with the limited facet size and island-relaxation observed in experiments. In addition, the relatively high rate of monomer diffusion on an island as well as the low barrier for interlayer diffusion are consistent with experimental observations that second-layer growth does not occur until after the first layer is complete. © *2015 AIP Publishing LLC.* [http://dx.doi.org/10.1063/1.4905144]

I. INTRODUCTION

The use of nanoparticle (NP) self-assembly to create ordered nanostructures is a topic of significant interest. One particular method which has been shown to lead to the formation of highly ordered nanocrystal monolayers[1–4] is the drop-drying of ligand-coated Au NPs in solution. In this method, a small toluene droplet which contains dodecanethiol (DDT) ligand coated NPs in solution is placed on a Si substrate and then allowed to evaporate in ambient conditions. As the toluene evaporates, the NPs are swept up and adsorbed at the toluene-air interface. They then diffuse and aggregate leading to the growth of two-dimensional islands with triangular packing which are defect-free and relatively compact. After the toluene has evaporated, a well-ordered monolayer of Au NPs is formed.

For a sufficiently large excess DDT concentration (corresponding to a large ligand density on each NP), the lifetime for NP desorption from the interface has been shown[3] to be significantly longer than the time for an adsorbed NP to diffuse and attach to another NP or island. As a result, the process of NP island nucleation and growth during drop-drying is very similar to epitaxial growth. Therefore, it is of interest to use the theoretical methods developed to analyze submonolayer island growth to study NP island self-assembly via drop-drying.

One concept which has proved useful in the analysis of epitaxial growth[5–12] is that of a critical island size i, corresponding to one less than the number of atoms or particles in the smallest stable island (see Fig. 1). In particular, standard nucleation theory[5,12] predicts that in the pre-coalescence regime, the submonolayer island density N depends on the critical island-size i and deposition flux F as $N \sim F^{\chi_i}$, where the exponent $\chi_i = i/(i+2)$ depends on the critical island-size. As a result, by measuring the dependence of the island-density on deposition flux, the critical island-size and NP interaction strength may be determined.

Recently, Joshi *et al.*[4] carried out a systematic study of submonolayer nucleation and growth during drop-drying, for NPs with three different Au core diameters ($d = 4.9 \pm 0.3$ nm, 6.0 ± 0.4 nm, and 8.0 ± 0.4 nm). In general, they found that the critical island-size decreases as the NP size increases. In particular, for 8.0 nm NPs, the critical island-size was found to be close to 2, corresponding to a stable trimer. In contrast, for 6.0 nm NPs, the critical island-size was found to be close to 6, corresponding to a stable heptamer. Finally, for the smallest NP size studied ($d = 4.9$ nm), a very large critical island-size (corresponding to $\chi \simeq 1$) was found. They also found that while the NP islands were relatively compact, the island relaxation was not sufficiently fast to eliminate the irregular island-shape due to coalescence. In addition, it was found that second layer growth did not begin until after the first layer was complete.

Here, we present the results of molecular dynamics (MD) and energetics calculations which we have carried out in order to understand these results. In particular, using an empirical potential[13] which takes into account the ligand-ligand and van der Waals interactions between NPs, we have investigated the dependence of the critical island-size on NP size, as well as the energy barriers for island-relaxation and interlayer diffusion. In good agreement with experiment, we find that the critical island-size increases with decreasing NP size, with values which are close to those obtained experimentally. In addition, our results for the barriers for edge-diffusion lead to values of the diffusion length which are consistent with the limited facet size and island-relaxation observed in experiments. The relatively small values obtained for the barriers for diffusion on an island and for interlayer diffusion are also consistent with the experimental observation that second-layer growth does not occur until the first layer is complete.

This paper is organized as follows. In Sec. II, we first describe the potential used in our simulations along with the methods used to study the dependence of the island stability on island-size and NP size, as well as the activation barriers

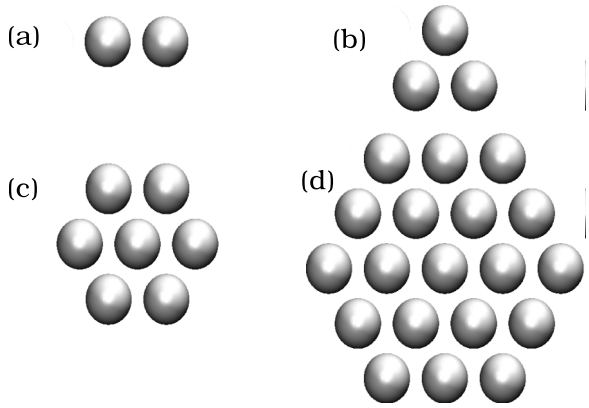

FIG. 1. Stable islands of size $i+1$ obtained assuming a bond-counting model with z nearest-neighbor bonds needed for stability. (a) $z = 1$, $i = 1$; (b) $z = 2$, $i = 2$; (c) $z = 3$, $i = 6$; (d) $z = 4$, $i = 18$.

and rates for island relaxation. We then present our results in Sec. III. Finally, we summarize our results in Sec. IV.

II. SIMULATIONS

In order to study the stability and relaxation of NP islands at room temperature, we have carried out constant temperature MD simulations. In our simulations, we have used an empirical potential which was developed by Khan *et al.*[13] to represent the interactions between dodecanethiol-coated Au NPs submerged in bulk toluene which takes into account the core-core van der Waals interaction as well as the ligand-ligand and ligand-toluene interactions. In order to take into account the temperature as well as the effects of damping[14] due to the viscosity of toluene, our simulations were carried out using Langevin dynamics[15] with a damping constant $B = 6\pi\eta r_h$ which depends on the viscosity of toluene η as well as the hydrodynamic radius ($r_h \simeq d/2 + 2.0$ nm) of the NP.

We note that in previous all-atom MD simulations[16] of a 6 nm NP adsorbed at the toluene-air interface, it was found[16] that due to the competition between ligand-solvent mixing (which tends to keep the NP below the interface) and the effects of surface tension, the NP remains primarily submerged below the interface. In addition, it was demonstrated,[16] in qualitative agreement with previous results[17] for alkanethiol-coated NPs in decane, that due to the relatively small ratio of the ligand length to the NP diameter, there is relatively little asymmetry or patchiness in the ligand coating. Accordingly, we expect that this potential should provide a reasonably accurate representation of the interaction between NPs adsorbed at the toluene-air interface.

While the details of this potential are discussed in Ref. 13, it is worth noting that there are two versions. One corresponds to a "non-denting" interaction in which it is assumed that there is significant interpenetration between the ligands from different NPs, while the other corresponds to a "denting" interaction in which the amount of ligand interpenetration is assumed to be negligible. Fig. 2 shows the corresponding pair-interaction $V(R)$ as a function of the distance R between the center of the NPs for all three NP sizes for both the denting and non-denting potentials. As can be seen, the depth of the potential well is greater for the denting potential than for the non-denting potential and also increases with increasing NP size. In addition, while the equilibrium pair-separation for the denting potential is slightly smaller than for the non-denting potential, both are in reasonable agreement with experiments. In particular, there is excellent agreement between the predicted and experimental values of the equilibrium pair-separation ($a = 96$ Å) for 8 nm NPs while for the smaller NP sizes, the predicted equilibrium pair-separations are only 5%-7% below the experimental values. Although not shown here, we note that the van der Waals interaction between the Au cores contributes approximately 30%-40% of the overall dimer binding energy. As a result, for the NP sizes considered here, the ligand-ligand and ligand-solvent interactions dominate.

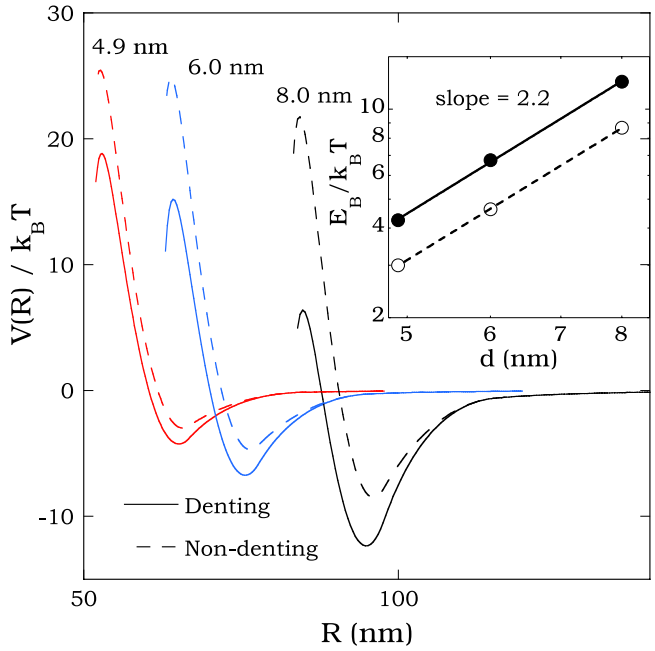

FIG. 2. Denting (solid lines) and non-denting (dashed lines) potential for all three NP sizes. Inset shows power-law dependence of dimer binding energy E_B on NP core diameter d.

As can be seen in Fig. 2, the potential of Khan *et al.* does not properly take into account steric effects related to the ligand-core interaction which become important at small separation R. In particular, rather than continuing to increase with decreasing separation for small R, the potential decreases. However, this artifact of the potential does not affect the binding energy at the equilibrium NP separation. In addition, since at the turning point, the peak in $V(R)/k_BT$ is relatively large at room temperature, this region of the potential is not likely to be accessed on the time-scale of our cluster stability simulations.

In order to study the stability of small compact NP clusters at room temperature, MD simulations were carried out to determine the typical NP detachment time as a function of cluster-size and NP size. In our simulations, a timestep $\Delta t = 0.05$ ps was used. We note that this value is less than 10^{-4} of a typical dimer oscillation period. In each case, the density of bulk gold combined with the NP diameter was used to estimate the NP mass. While the potential of Khan *et al.*[13] was used to describe the NP-NP interactions, a quadratic potential $V(z) = \frac{1}{2}\kappa z^2$ (where z is the height of the NP above

its equilibrium position at the interface) was used to represent the interaction of the NPs with the interface. Here, the value $\kappa \simeq 0.004$ eV/Å^2 was estimated based on previous all-atom molecular dynamics simulations[16] for a 6 nm NP at the toluene-air interface. We note that in our multilayer simulations, this potential was only applied to the NPs in the first layer.

In these simulations, averages were taken over 100 runs, while a NP was assumed to detach if its distance l_{det} to the closest NP was equal to or larger than 1.9 a, where a is the equilibrium pair-separation as determined by the Khan *et al.* potential. We note that at this distance, the pair-interaction is negligible. As a result, and as discussed in more detail in Sec. III, the corresponding detachment times are relatively insensitive to the specific value of l_{det}. We note that l_{det} is also close to but slightly larger than the second nearest-neighbor distance on a triangular lattice with lattice constant a and so corresponds to a typical detachment distance in a lattice model.

In addition to using MD simulations to study island stability, we have also calculated activation energies for a variety of important island relaxation mechanisms, such as edge-diffusion, trimer "opening," dimer shearing, and corner rounding, as well as for a variety of other relaxation mechanisms of importance in multilayer growth including monomer diffusion on top of an island, monomer desorption from an island, and interlayer diffusion. While many of our activation energy calculations were carried out using the nudged-elastic band (NEB)[18,19] method, in some cases, it was found more convenient to use the drag method.[20] In order to verify the accuracy[21,22] of the simpler drag method, several barriers were calculated using both methods. We note that typically the drag method involves the use of an initial path which is based on a linear interpolation between the initial and final minimized states. However, to avoid the unphysical small-distance region of the potential, in some cases, a quadratic interpolation was used for the initial path.

III. RESULTS

A. Island stability

As shown in Table I, in order to determine the critical island size for the nucleation and growth of submonolayer NP islands, we have calculated the average detachment time τ_{det} as a function of NP size for the dimer, trimer, heptamer, and 19-mer clusters shown in Fig. 1, as well as for a 37 NP island (corresponding to a central NP surrounded by four hexagonal rings of NPs) for both the denting and non-denting potentials. Also shown in Table I are the experimentally determined monomer attachment times $\tau_{att}^{expt} = N/F$ (where N is the island density in monolayers (ML) and F is the deposition flux in ML/s) corresponding to the average time-interval between two successive monomer attachments to a particular island. For comparison, the typical time $\tau_{diff} \simeq (l_{det} - a)^2/4D_m$ for a monomer to diffuse to a distance equal to the detachment distance l_{det} is also shown. We note that here we have assumed, in good agreement with previous all-atom MD simulation results[16] for the diffusion of a 6 nm NP at the toluene-air interface, that the monomer diffusion coefficient is given by the Stokes-Einstein expression $D_m = k_B T/6\pi\eta r_h$, where k_B is Boltzmann constant. As can be seen, in all cases for which $\tau_{det} \gg \tau_{att}^{expt}$, τ_{diff} is orders of magnitude smaller than the monomer attachment time. This demonstrates that for stable islands, the detachment time is not sensitive to the exact value of the detachment distance (l_{det}) used. In addition, for all NP and island sizes, the detachment times obtained using the denting potential are significantly longer than obtained using the non-denting potential. We now compare our results with the corresponding experimental results for the critical island-size in submonolayer island nucleation and growth for all three NP sizes.

We first consider the case of 8.0 nm NPs for which the experimentally estimated critical island-size was found to be between 1 and 2 ($i = 1.6$). In good agreement with this estimate, the dimer detachment time ($\tau_{det} = 25.9$ μs) for the non-denting potential is significantly smaller than the corresponding experimental attachment time (144 μs), thus indicating that dimers are not stable. However, for the same potential, the trimer detachment time ($\tau_{att} = 1378$ μs) is significantly higher than τ_{att}. This implies that islands of size 3 and larger are more likely to grow than to shrink, and that as a result, the critical island-size is close to 2, in reasonable agreement with experiment. In contrast, the denting potential leads to an average detachment time for a dimer which is significantly longer than the experimental monomer attachment time, thus implying a critical island size of 1, in disagreement with the experimental estimate.

TABLE I. Detachment times as function of island size and NP diameter d for both denting (D) and non-denting (ND) potentials. Top row indicates island size. Two right columns show experimental monomer-island attachment time τ_{att}^{expt} and estimated monomer diffusion time τ_{diff} (see text) in μs. Detachment times in boldface correspond to values which are significantly larger than the corresponding experimental attachment times (also shown in boldface), thus indicating that islands of that size are stable.

		Detachment time (μs)						
d (nm)	Potential	2	3	7	19	37	τ_{att}^{expt} (μs)	τ_{diff} (μs)
4.9	D	0.79	1.1	2.5	7.1	6.2	**50**	0.20
	ND	0.30	0.38	0.43	0.45	...	50	0.21
6.0	D	7.00	46.55	**687**	...	...	**97**	0.32
	ND	0.87	1.8	6.5	19.5	...	97	0.33
8.0	D	>1000	...	...	...	...	144	0.62
	ND	25.9	**1378**	...	...	...	**144**	0.64

We now consider the case of 6.0 nm NPs for which the experimental results indicate a somewhat larger critical island-size ($i \simeq 4.7$) corresponding to $\chi \simeq 0.7$. In this case, our denting potential simulation results indicate that the heptamer, which corresponds to the smallest island for which all NPs have at least 3 bonds, is the smallest stable island. This implies a critical island-size of 6 corresponding to $\chi \simeq 0.75$, in relatively good agreement with experiment. In contrast, for the non-denting potential, the critical island-size is significantly larger since even 19-mers are not stable on the time-scale corresponding to monomer attachment. Thus, in contrast to the case of 8.0 nm NPs, for 6.0 nm NPs, the denting potential appears to give better agreement with experiments than the non-denting potential.

Finally, we consider the case of 4.9 nm NPs for which the experimental value of χ is close to 1, thus indicating a very large critical island-size. In this case, both the denting and non-denting potentials are in reasonable qualitative agreement with experiment since they both indicate that even relatively large clusters are not stable on the monomer attachment time-scale.

These results demonstrate that the potential of Khan *et al.* is consistent with the experimental results for all three NP sizes. However, they also indicate that for the large NP size ($d = 8.0$ nm), the non-denting potential gives better agreement with experiment. In contrast, for the two smaller NP sizes (4.9 and 6.0 nm), the denting potential gives better agreement with experiment. Assuming a constant ligand density for all three NP sizes,[23] one possible explanation for this difference is the dependence of the radius of curvature on NP size. In particular, we expect that the relatively small radius of curvature for small NPs may enhance the misalignment of ligands on neighboring NPs, thus inhibiting interpenetration, which is consistent with the denting potential. In contrast, for 8.0 nm NPs, the larger radius of curvature may lead to better alignment thus allowing more ligand interpenetration, as is assumed by the non-denting potential.

We note that damping due to toluene plays an important role in determining the detachment times and stability of small clusters, since the oscillation period τ of a NP attached to an island[24] is significantly longer than the typical damping time τ_{damp} for a single NP in toluene (25-75 ps depending on the NP size). As a result, the oscillations of a NP in an island are overdamped and the detachment times obtained in our simulations are significantly longer than expected in the absence of damping. In particular, the detachment time for a dimer in the absence of damping may be estimated using the expression $\tau_{det}^{nodamp} \simeq \exp(E_b/k_BT)/f$, where E_b is the dimer (pair) binding energy (see Table II) and the oscillation frequency $f = \frac{\sqrt{2}}{2\pi}\sqrt{\frac{K}{M}}$, where K is the spring constant for the potential and M is the NP mass.

As an example, for 6 nm NPs with a denting potential, the detachment time obtained in our simulations ($\tau_{det} = 7$ μs) is significantly longer than the corresponding estimate (0.44 μs) obtained using the expression above. Similarly, an estimate of the detachment rates for dimers and trimers which takes into account the activation barriers for one-bond and two-bond detachment (see Table II) as well as the existence of different single-step and multi-step modes for trimer break-up (see Sec. III B) suggests that in the absence of damping due to toluene (and ignoring any increase in the relevant prefactors due to the increase in the number of bonds), the rate of trimer break-up should be approximately 100 times slower than the rate of dimer break-up for the 6 nm NP with a denting potential. However, the corresponding ratio obtained in our simulations (approximately 7) is significantly smaller. This may be partially explained by an increase in the relevant prefactors due to the increase in the number of bonds. However, it is also due to the fact that the degree of overdamping (corresponding to the ratio τ/τ_{damp} of the oscillation period to the damping time) is reduced for trimers since the two-bond oscillation period is significantly smaller than the dimer oscillation period. A similar analysis, which again takes into account the increase in the number of detachment modes with increasing island-size, along with the corresponding increase in the relevant prefactors as well as the decreased effects of damping may also explain the relatively small ratio of the heptamer and trimer detachment times.[25]

B. Island relaxation

We now consider the mechanisms for island relaxation since they play an important role in determining the island morphology. As can be seen in Fig. 3, while small islands are relatively compact, larger islands are somewhat irregular due to the effects of island coalescence combined with limited relaxation. In order to investigate the corresponding relaxation mechanisms, we have calculated the activation energies for the processes of dimer shear, trimer opening, edge-diffusion, and corner-rounding (see Fig. 4). For each NP size and potential,

TABLE II. Energy barriers for pair breaking, edge-diffusion, corner-rounding, trimer-opening, and dimer shear. Right half of the table shows monomer diffusion rate D_m, edge-diffusion rate D_e, and critical length-scale l_c.

		Energies							
d (nm)	Potential	Pair (eV)	Edge (eV)	Corner (eV)	Trimer (eV)	Shear (eV)	D_m (μm^2/s)	D_e (μm^2/s)	l_c (μm)
4.9	D	0.11	0.11[a]	0.11	0.11	0.22[a]	84.6	48.5	0.17
	ND	0.072	0.074	0.077	0.077	0.15	84.6	46.6	0.17
6.0	D	0.17	0.17	0.18	0.17	0.34	73	2.9	0.06
	ND	0.12	0.117	0.12	0.12	0.24	73	21.4	0.16
8.0	D	0.31	0.31	0.32	0.32	0.63	58.4	3.4	0.08
	ND	0.21	0.21	0.22	0.22	0.43	58.4	0.6	0.03

[a]Measured using both NEB and drag-methods.

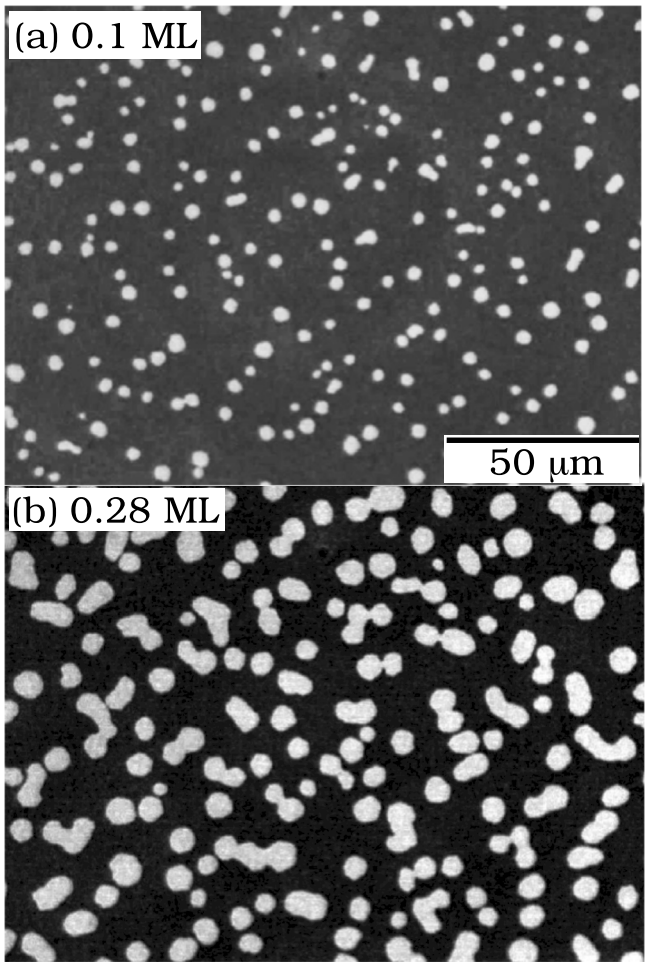

FIG. 3. Pictures of 6.0 nm NP islands obtained in drop-drying experiments at a coverage of 0.1 ML (a) and 0.28 ML (b). Reprinted with permission from Joshi *et al.*, Phys. Rev. E **90**, 032406 (2014). Copyright 2014 American Physical Society.

the corresponding activation energies are shown in Table II. The pair binding energies are also shown for comparison.

As can be seen in Table II, for a given NP size, the barriers for edge-diffusion, corner-rounding, and trimer opening are all approximately equal and have values which are close to those for single-bond (pair) detachment. This indicates that these barriers can be accurately calculated by counting the number of broken bonds. The relatively small values of the barriers for the 4.9 and 6.0 nm denting and non-denting potentials, as well as for the 8.0 nm non-denting potential also indicate that all three of these processes will be quite active at room temperature, thus promoting detachment and island rearrangement. The good agreement between the barrier for corner rounding and that for edge-diffusion also indicates that there is no 2D "kink" Ehrlich-Schwoebel (ES) barrier[26–28] which can lead to a morphological instability.

We now consider the effects of dimer shear and trimer-opening on small cluster stability. While trimer break-up can occur directly via a two-bond breaking process, it can also occur via a multistage process involving two consecutive moves, e.g., trimer opening followed by detachment, which involve the breaking of a single-bond. A detailed analysis indicates that inclusion of this process triples the overall break-up rate compared to the case in which such multistage processes are not included. Similarly, dimer shear (see Fig. 4(a)) can significantly enhance the rate of detachment from a heptamer since this requires breaking two bonds rather than three. This leads to a multi-stage pathway for detachment which involves dimer shear followed by trimer opening and detachment rather than breaking all three bonds in a single step. As a result, the corresponding total detachment rate is approximately three times larger than it would be in the absence of such multistage processes.

While dimer shear and trimer-opening play an important role in determining the stability of small clusters, the processes of edge-diffusion and corner-rounding play a crucial role in determining the island morphology. Since there is no extra barrier to corner diffusion, the characteristic length-scale for smoothing via edge-diffusion may be estimated as $l = \sqrt{2D_e\tau_l}$, where D_e is the rate of edge-diffusion and τ_l is the average time an edge-diffuser can diffuse before another monomer attaches within a length l. Assuming circular islands of radius r, the typical time between two monomer attachments to the same island within a distance l may be approximated as $\tau_l = 2\pi r N/lF$. Setting the diffusion length l equal to a typical island radius r leads to the following expression for the characteristic length-scale l_c for smoothing via edge-diffusion:

$$l_c = (4\pi D_e N/F)^{1/2}. \quad (1)$$

Since damping may play an important role, in order to directly determine the rate of edge-diffusion D_e, we have also carried out MD simulations for each NP size. In each case, D_e was determined by averaging the hopping time for an edge-diffuser over 100 events. Table II shows the corresponding values for D_e along with the corresponding characteristic length-scale l_c for smoothing via edge-diffusion obtained using Eq. (1). As can be seen, l_c is typically of the order of 0.2 μm or smaller. While additional mechanisms for smoothing such as detachment may also play a role, this is consistent with the limited facet size and island-relaxation observed in experiments.

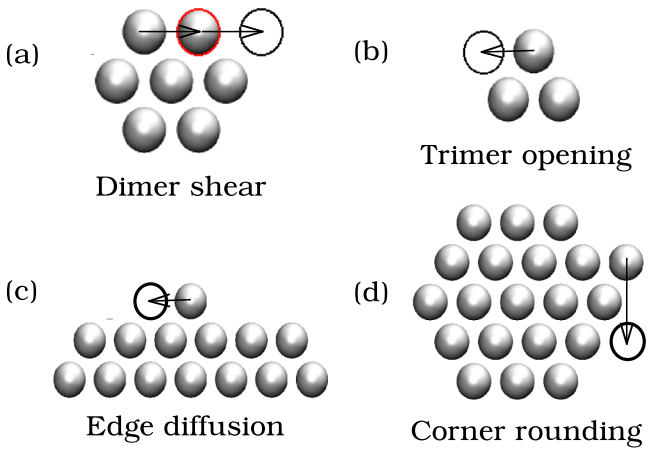

FIG. 4. Schematic showing transitions listed in Table II. (a) Dimer shear, (b) trimer opening, (c) edge diffusion, and (d) corner rounding.

TABLE III. Activation barriers for motion on a NP island including monomer hopping (E_I), the Ehrlich-Schwoebel barrier for interlayer diffusion (E_{ES}), and the barrier E_{des} for monomer desorption.

d (nm)	Potential	E_I (eV)	E_{ES} (eV)	E_{des} (eV)	ν_I (Hz)	D_I (μm^2/s)	l_{des} (μm)
4.9	D	0.094	0.007	0.34	2.1×10^8	103.9	1.3
	ND	0.065	0.015	0.24	1.5×10^8	242.3	0.3
6.0	D	0.16	0.02	0.53	6.7×10^8	31.9	17.6
	ND	0.11	0.02	0.37	2.2×10^8	79.9	2.0
8.0	D	0.30	0.03	0.97	6.5×10^{10}	18.1	8877
	ND	0.20	0.03	0.67	1.4×10^9	21.5	164.5

C. Multilayer growth

In addition to the mechanisms of two-dimensional island growth and relaxation, it is also of interest to consider the mechanisms for multilayer growth. Surprisingly, experimental results[4] indicate that there is no second layer growth in the submonolayer regime even at large coverage. In order to understand this, we have calculated the activation barrier E_I for monomer hopping on top of an island, along with the barrier E_{des} for monomer desorption from an island, as well as the Ehrlich-Schwoebel barrier E_{ES} for interlayer diffusion (where E_{ES} is the difference between the barrier for interlayer diffusion and E_I). Since damping plays a role and it is difficult to accurately calculate the effective monomer hopping rate based solely on the activation barrier, we have also directly measured the diffusion rate D_I corresponding to monomer hopping on an island. The corresponding results are shown in Table III.

As can be seen from Fig. 5(a), since the mechanism for monomer diffusion on an island involves breaking a single bond and passing through a bridge site, the corresponding barriers are relatively low and are similar to those obtained in Sec. III B for edge-diffusion. In addition, using the results for D_I shown in Table III along with the expression $l_{diff} = \sqrt{4D_I/F}$ for the typical distance a monomer can diffuse before another monomer lands on top of it, and typical experimental deposition rates $F = 10^{-5} - 10^{-2}$ ML/s leads to values for the diffusion length which are significantly larger than a typical island-size in experiments. This indicates that the only limiting factor for second layer growth is the possible existence of a barrier to interlayer diffusion.

Table III shows our results for the ES barrier E_{ES} for all three NP sizes both with and without denting. As can be seen, in all cases the ES barrier is of the order of k_BT or smaller. This implies that there is essentially no additional barrier for a NP to diffuse to the layer below. Combined with the large diffusion length, this result supports the experimental observation that second layer growth does not occur until the first layer is complete.

Finally, we consider the barrier E_{des} for the desorption of a NP from an island. As can be seen in Table III, E_{des} is approximately three times larger than the energy of a single bond. Assuming the desorption prefactor ν_{des} is the same as that for monomer hopping on an island, the desorption time $\tau_{des} = \nu_I^{-1}\exp(E_{des}/kT)$ may be estimated. The distance $l_{des} = (4D_I\tau_{des})^{1/2}$ that a monomer deposited on an island can diffuse before desorbing can then be calculated. As can be seen, for the 6 nm denting potential and both 8 nm potentials, the corresponding values of l_{des} (18 μm and 165 μm, respectively) are comparable to or larger than the typical island-size observed in experiments. This result is consistent with the experimentally observed linear behavior[3,4] for the time-dependence of the coverage, since assuming a large diffusion length for NPs at the toluene-air interface, it implies a capture zone which is independent of the island-size. In contrast, for the 4.9 nm denting potential, the estimated diffusion length is significantly smaller. This suggests that in this case, desorption from islands may play a role at high coverage.

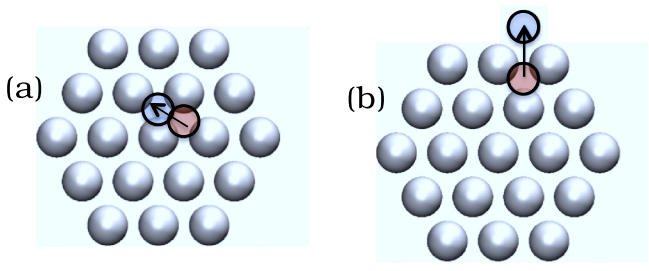

FIG. 5. Schematic showing two possible transition pathways for a monomer on a NP island: (a) Monomer hopping and (b) interlayer diffusion.

IV. DISCUSSION

In order to explain the results of recent experiments on Au NP island self-assembly in toluene, we have carried out molecular dynamics and energy barrier calculations using an empirical potential which takes into account the ligand-ligand, ligand-solvent, and van der Waals interactions. In particular, we have investigated the dependence of the critical island-size on NP size and have also calculated the energy barriers for island-relaxation, interlayer diffusion, and island desorption.

In good agreement with experiment, we find that the critical island-size increases with decreasing NP size. This is consistent with the strong dependence of the single-bond binding energy on NP size. In particular, for the 8 nm NP, our MD simulation results for the non-denting potential indicate that the critical island-size is equal to 2, in reasonable agreement with the experimental estimate $i \simeq 1.6$. Similarly, for the 6.0 nm NP, the denting potential indicates that heptamers are stable. This corresponds to a critical island-size $i \simeq 6$, which implies a value of the flux exponent $\chi \simeq 0.75$ which is also in reasonable agreement with experiments. Finally, for the 4.9 nm NP, both the non-denting and denting potential results indicate a very large critical island-size, in good agreement with experiments.

While these results demonstrate that the potential of Khan *et al.* is consistent with experimental results for all three NP sizes, they also indicate that while the denting potential is appropriate for small NP sizes, the non-denting potential may be more appropriate for larger NP size. Assuming a constant ligand density,[23] one possible explanation is the dependence of the radius of curvature on NP size. In particular, we expect that the relatively small radius of curvature for small NPs may enhance the misalignment of ligands on neighboring NPs, thus inhibiting interpenetration, which is consistent with the denting potential. In contrast, for 8.0 nm NPs, the larger radius of curvature may lead to better alignment thus allowing more ligand interpenetration, as is assumed by the non-denting potential.

In this connection, it is worth noting that in the paper of Khan *et al.*,[13] the non-denting potential was preferred over the denting potential due to the fact that for a decanethiol ligand attached to a 5 nm core-diameter NP, the denting potential was found to remain negative at small NP separation. However, this effect does not occur for the case of the dodecanethiol ligands considered here. Furthermore, it is not surprising that both the denting and non-denting potentials would underestimate the potential energy at small NP separations since although they include an elastic contribution due to entropy, they do not take into account additional elastic contributions which become important at small length-scales. We note that in our simulations this range of small particle separations is not explored at room temperature, and so there is no need to include these additional contributions.

In addition to the MD simulations which we have carried out to determine the dependence of the critical island-size on NP size, we have also calculated the activation energies for a variety of different relaxation mechanisms. In general, and as shown in the inset of Fig. 2, we find that the single-bond (dimer) binding energy increases approximately as the square of the NP diameter. This is consistent with our expectation that, for this range of NP sizes, the ligand-ligand interaction dominates and is proportional to the NP surface area. However, the van der Waals interaction also accounts for approximately 30%-40% of the pair binding energy. In addition, our results indicate that a simple bond-counting model, in which the barrier is assumed to be proportional to the number of broken bonds, may be used to accurately estimate the activation energies for different processes. As a result, multistage processes which include collective moves such as dimer shear, along with other processes such as trimer opening, can significantly enhance the overall detachment rate for small clusters.

For the case of edge-diffusion along a straight edge, our calculations indicate that the activation barriers are relatively low, ranging from 0.1 eV for the 4.9 nm denting potential to 0.2 eV for the 8.0 nm non-denting potential, while there is no extra barrier to corner-rounding. As a result, we expect that edge-diffusion will play a significant role in island-relaxation, in addition to monomer attachment/detachment. We have also derived an expression for the critical length-scale for smoothing via edge-diffusion during island growth. Using this expression along with our MD results for the rate of edge-diffusion leads to an estimate of the critical length-scale for smoothing via edge-diffusion during island growth which is consistent with the limited facet size and island-relaxation observed in experiments.

Finally, in order to understand the key mechanisms involved in multilayer growth, we have also calculated the Ehrlich-Schwoebel barrier for interlayer diffusion as well as the activation barriers for monomer hopping and/or desorption from an island. In all cases, the ES barrier was found to be of the order of k_BT or smaller, thus implying a minimal additional barrier for a NP to diffuse to the layer below. Combined with our MD results for the rate of monomer hopping on an island, these results are consistent with the experimental observation that second layer island growth does not occur until after the first layer is complete. In addition, for both 6.0 nm NPs with the denting potential as well as 8.0 nm NPs, the average distance l_{des} that a monomer may hop on an island before desorption was found to be significantly longer than the typical island-size. As discussed in Ref. 3, these results are consistent with experimental observations of linear behavior for the growth of the submonolayer island coverage with time. In contrast, for 4.9 nm NPs, the desorption length l_{des} was found to be somewhat smaller, which may imply nonlinear behavior[3] for the dependence of the island coverage on time at high coverages.

In conclusion, our MD simulation and activation energy results indicate that the potential of Khan *et al.*[13] is consistent with experimental results for the critical island-size, submonolayer island-morphology, and multilayer growth for all three NP sizes. In particular, good agreement with experiments is obtained with the use of the non-denting potential for the 8.0 nm NPs, while for the smaller 4.9 nm and 6.0 nm NPs, the denting potential leads to better agreement. In the future, it would be of interest to use our results for the corresponding island detachment, relaxation, and interlayer diffusion rates as a function of NP size in order to carry out kinetic Monte Carlo simulations of NP island self-assembly on experimental time-scales.

ACKNOWLEDGMENTS

This work was supported by the National Science Foundation under Grant Nos. CHE-1012896 and DMR-1410840. We also acknowledge a grant of computer time from the Ohio Supercomputer Center.

[1]X.-M. Lin, H. M. Jaeger, C. M. Sorensen, and K. J. Klabunde, J. Phys. Chem. B **105**, 3353 (2001).
[2]S. Narayanan, J. Wang, and X.-M. Lin, Phys. Rev. Lett. **93**, 135503 (2004).
[3]T. P. Bigioni, X.-M. Lin, T. T. Nguyen, E. I. Corwin, T. A. Witten, and H. M. Jaeger, Nat. Mater. **5**, 265 (2006).
[4]C. P. Joshi, Y. Shim, T. P. Bigioni, and J. G. Amar, Phys. Rev. E **90**, 032406 (2014).
[5]J. A. Venables, G. D. Spiller, and M. Hanbücken, Rep. Prog. Phys. **47**, 399 (1984).
[6]J. A. Stroscio and D. T. Pierce, Phys. Rev. B **49**, 8522 (1994).
[7]A. R. Avery, H. T. Dobbs, D. M. Holmes, B. A. Joyce, and D. D. Vvedensky, Phys. Rev. Lett. **79**, 3938 (1997).
[8]Y. Ebiko, S. Muto, D. Suzuki, S. Itoh, K. Shiramine, T. Haga, Y. Nakata, and N. Yokoyama, Phys. Rev. Lett. **80**, 2650 (1998).
[9]H. Brune, G. S. Bales, J. Jacobsen, C. Boragno, and K. Kern, Phys. Rev. B **60**, 5991 (1999).
[10]H. Zheng, M. H. Xie, H. S. Wu, and Q. K. Xue, Phys. Rev. B **77**, 045303 (2008).
[11]F. Arciprete, E. Placidi, V. Sessi, M. Fanfoni, F. Patella, and A. Balzarotti, Appl. Phys. Lett. **89**, 041904 (2006).
[12]J. W. Evans, P. A. Thiel, and M. C. Bartelt, Surf. Sci. Rep. **61**, 1 (2006).

[13]S. J. Khan, F. Pierce, C. M. Sorensen, and A. Chakrabarti, Langmuir **25**, 13861 (2009).
[14]D. K. Ermak and H. Buckholz, J. Comput. Phys. **35**, 169 (1980).
[15]N. Gronbach-Jensen and O. Farago, Mol. Phys. **111**, 983 (2013).
[16]N. N. Poddar and J. G. Amar, J. Chem. Phys. **140**, 244702 (2014).
[17]J. M. D. Lane and G. S. Grest, Phys. Rev. Lett. **104**, 235501 (2010).
[18]H. Jónsson, G. Mills, and K. W. Jacobsen, in *Classical and Quantum Dynamics in Condensed Phase Simulations*, edited by B. J. Berne, G. Ciccotti, and D. F. Coker (World Scientific, Singapore, 1998), p. 385.
[19]G. Henkelman, B. P. Uberuaga, and H. Jónsson, J. Chem. Phys. **113**, 9901 (2000).
[20]Z.-H. Huang and R. E. Allen, J. Vac. Sci. Technol., A **9**, 876 (1991).
[21]T. A. Halgren and W. N. Lipscomb, Chem. Phys. Lett. **49**, 225 (1977).
[22]M. J. Rothman and L. L. Lohr, Chem. Phys. Lett. **70**, 405 (1980).
[23]G. H. Woehrle, L. O. Brown, and J. E. Hutchison, J. Am. Chem. Soc. **127**, 2172 (2005).
[24]Depending on the NP size, the natural oscillation period $\tau = 1/f$ for a dimer ranges from 500 ps to 1000 ps.
[25]To further understand the effects of damping on the detachment time, we have carried out additional simulations for an 8 nm NP dimer, 6 nm NP trimer, and 4.9 nm NP 19-mer in which the ratio $\alpha = \tau/\tau_{damp}$ was varied by an order of magnitude. As expected, in all cases we found that the detachment time increased with increasing α and was approximately proportional to this ratio.
[26]G. Ehrlich and F. G. Hudda, J. Chem. Phys. **44**, 1039 (1966).
[27]R. L. Schwoebel and E. J. Shipsey, J. Appl. Phys. **37**, 3682 (1966).
[28]O. Pierre-Louis, M. R. D'Orsogna, and T. L. Einstein, Phys. Rev. Lett. **82**, 3661 (1999).